

# Light-Induced Static Magnetization: Nonlinear Edelstein Effect

Haowei Xu <sup>1</sup>, Jian Zhou <sup>1</sup>, Hua Wang <sup>1</sup>, and Ju Li <sup>1,2</sup> <sup>†</sup>

<sup>1</sup> Department of Nuclear Science and Engineering, Massachusetts Institute of Technology,  
Cambridge, Massachusetts 02139, USA

<sup>2</sup> Department of Materials Science and Engineering, Massachusetts Institute of Technology,  
Cambridge, Massachusetts 02139, USA

## Abstract

We theoretically and computationally demonstrate that static magnetization can be generated under light illumination via nonlinear Edelstein effect (NLEE). NLEE is applicable to semiconductors under both linearly and circularly polarized light, and there are no constraints from either spatial inversion or time-reversal symmetry. Remarkably, magnetization can be induced under linearly polarized light in nonmagnetic materials. With *ab initio* calculations, we reveal several prominent features of NLEE. We find that the orbital contributions can be significantly greater than the spin contributions. And magnetization with various orderings, including anti-ferromagnetic, ferromagnetic, etc., are all realizable with NLEE, which may facilitate many applications, such as unveiling hidden physical effects, creating a spatially varying magnetization, or manipulating the magnetization of anti-ferromagnetic materials. The relationship between NLEE and other magneto-optic effects, including the inverse Faraday effect and inverse Cotton-Mouton effect, is also discussed.

---

<sup>†</sup> correspondence to: [liju@mit.edu](mailto:liju@mit.edu)

**Introduction.** The generation and manipulation of magnetization is the central issue in magnetic information storage and spintronics<sup>1,2</sup>. Conventionally, one uses the external magnetic field to read and write magnetism. However, since the magnetic coupling is weak, one usually needs a large magnetic field. For example, recent experimental works show that  $\sim 1$  T magnetic field is required to flip the CrI<sub>3</sub> bilayer from anti-ferromagnetic into ferromagnetic ordering<sup>3</sup>. Furthermore, it is hard to confine or focus a magnetic field. Modern spintronics requires fast and precise control over magnetization, and one has to resort to electrical or optical approaches. It has been demonstrated that electrical or optical fields with moderate strength could induce relatively larger effective magnetic field, which could control magnetism efficiently via photonic coupling. For example, the Edelstein effect<sup>4-7</sup> converts charge current to spin accumulation, and spin-transfer torque<sup>8</sup> uses a spin-polarized current to modify the magnetization, where the spin-polarized current can be generated electrically<sup>9-12</sup> or optically<sup>13,14</sup>. Optical approaches can also be used to reorient magnetization through the inverse Faraday effect (IFE)<sup>15,16</sup> or inverse Cotton-Mouton effect (ICME)<sup>17-19</sup>.

In this work, we generalize the linear Edelstein effect (LEE) into the second-order nonlinear Edelstein effect (NLEE). Compared with LEE, which is an *intra-band* process and needs to be applied to metals, NLEE has *inter-band* contributions and can be used in semiconductors and insulators. We find that the NLEE can induce a larger effective magnetic field than that of LEE at moderate electric field strength ( $E \gtrsim 10$  MV/m). In addition, from symmetry considerations, NLEE is not constrained by either spatial inversion  $\mathcal{P}$  or time-reversal  $\mathcal{T}$  symmetry, whereas LEE vanishes in  $\mathcal{P}$ -conserved systems. Hence, NLEE can be active in a lot of materials. Notably, magnetization can be generated under linearly polarized light (LPL) in nonmagnetic materials, and we attribute this effect to the breaking of  $\mathcal{T}$  by energy dissipation. Furthermore, as an opto-magnetic effect, NLEE enjoys many salient merits of optical approaches, as it can be non-contact, non-invasive, and ultrafast. These factors render NLEE a potentially effective method for generating and manipulating magnetization.

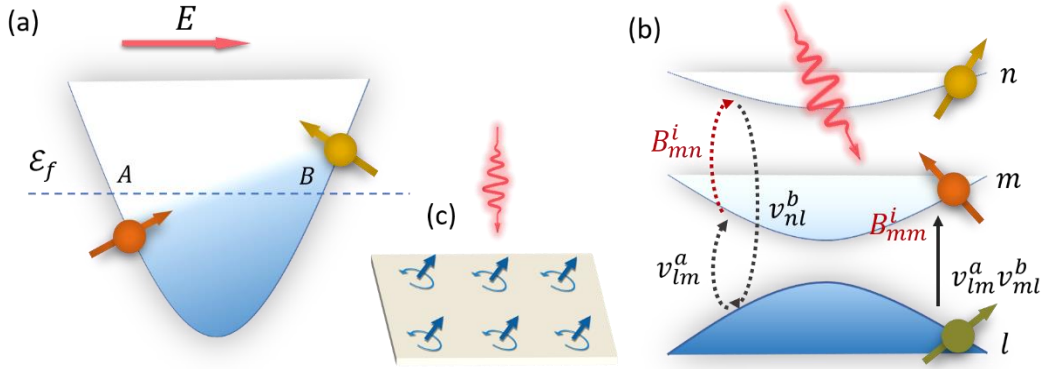


**Figure 1.** Simplified physical pictures of (a) LEE and (b) NLEE. The blue filling indicates electron occupation. For LEE, the static electric field modifies electron distribution in a single band (intra-band process). For NLEE, light excites interband transitions. The three-band process in Eq. (2) is illustrated by the dashed arrows on the left side of (b), while the two-band process in Eq. (4) is illustrated by the solid arrow on the right side. (c) Local vortices in the photocurrent (blue) and the associated orbital magnetization (blue) under light (red) illumination.

In order to quantitatively illustrate the properties of NLEE, we perform *ab initio* calculations in different material systems, including non-magnetic transition metal dichalcogenides (TMD, e.g. MoTe<sub>2</sub>) and antiferromagnetic CrI<sub>3</sub> bilayers. We incorporate orbital magnetic as well as conventional spin magnetic moments. Remarkably, we find that the orbital contribution can be stronger than the spin contribution, especially in nonmagnetic systems. In bilayer MoTe<sub>2</sub>, the NLEE is sensitive to its van der Waals (vdW) stacking order, and various opto-magnetic orderings, including anti-ferromagnetic (AFM) and ferro-magnetic (FM), are achievable and controllable. Interestingly, we also find that the hidden spin polarization<sup>20</sup> in non-magnetic materials can emerge when the system is driven out of equilibrium. Such methodology may be applied to detect and measure other hidden physical effects as well. Finally, we discuss the possibility of switching the AFM ordering in CrI<sub>3</sub> bilayer with NLEE, making use of the spatially varying magnetization. The relationship between NLEE and IFE and ICME is also addressed. The strength of the magnetization generated by NLEE depends linearly on the light intensity, and can be detected by quantum sensors<sup>21</sup> such as SQUID, NV centers, etc., even if the light intensity is mild.

**Mechanisms and Theory.** Generally speaking, the electron magnetic moment  $m$  has both the spin ( $S$ ) and orbital ( $L$ ) angular momentum contributions,  $m = \mu_B(2S + L)$ , where the factor of 2 for  $S$  is the g-factor of the electron spin. The total magnetization of an electron ensemble can be written as  $M = \text{Tr}[m\rho]$ , where  $\rho$  is the density matrix. For example, in nonmagnetic materials, one has

$M_0 = \text{Tr}[m\rho_0] = 0$ , where  $\rho_0$  is the equilibrium density matrix. In magnetic materials (spin polarized or orbital polarized, or both), the exchange interaction induces a finite spontaneous magnetization  $M_0$ . When the electrons are driven out of equilibrium, an additional magnetization  $\delta M = \text{Tr}[m\delta\rho]$  arises, where  $\delta\rho$  is the perturbation in the density matrix. For the spin part, a nonzero  $\delta M^S = 2\mu_B \text{Tr}[S\delta\rho]$  requires that each electron has a specific spin polarization (a spin texture), which could be created by, e.g., spin-orbit coupling (SOC) and magnetic ordering. For the orbital part, since the orbital texture is ubiquitous in multi-orbital systems, a nonzero  $\delta M^L = \mu_B \text{Tr}[L\delta\rho]$  generally exists.

Various approaches can drive the electrons out of equilibrium, thus changing the magnetic state. A well-known mechanism is the LEE<sup>4-7</sup>: a static magnetization  $M^i = \zeta_a^i E^a$  is generated by a static electric field  $E^a$ , and  $\zeta_a^i$  is the response function. Here  $E^a$  modifies the density matrix as  $\delta\rho_E(\mathbf{k}) = \frac{e\tau E^a}{\hbar} \frac{\partial\rho_0}{\partial k^a}$  in the reciprocal space, where  $\tau$  is the carrier relaxation time, and  $k$  is the crystal momentum. This effect is schematically illustrated in Figure 1a: Region  $A$  ( $B$ ) of the Brillouin zone (BZ) will have fewer (more) electrons under  $E$ , which tilts the Fermi surface. If electrons in  $A$  and  $B$  have different spin/orbital polarizations, a net magnetization change ( $\delta M$ ) would arise. Hence, the LEE is an *intra*band process and only electrons near the Fermi level ( $\frac{\partial\rho_0}{\partial k^a} \neq 0$ ) contribute to it – thus the LEE applies only to metals.

We now generalize the LEE from static electric field to optical alternating electric field and discuss the second-order NLEE. Unlike a static electric field, light can induce electronic *inter*band transitions. According to nonlinear optics theory, light could induce a static magnetic moment

$$\delta M^{i,B} = \sum_{\Omega=\pm\omega} \chi_{ab}^{i,B}(0; \Omega, -\Omega) E^a(\Omega) E^b(-\Omega) \quad (1)$$

Here  $a, b$  and  $i$  indicate the directional component of the electric field and the magnetization, respectively.  $E(\omega)$  is the Fourier component of the electric field with angular frequency  $\omega$ .  $\chi_{ab}^{i,B}(0; \omega, -\omega)$  is the nonlinear response tensor. Superscript  $B$  indicates either spin ( $B = S$ ) or orbital ( $B = L$ ) degree of freedom, and a total magnetic moment is  $\delta M^{i,T} = \delta M^{i,S} + \delta M^{i,L}$ . The formula of  $\chi_{ab}^{i,B}$  can be obtained from quadratic response theory<sup>13,22-24</sup> (Supplementary Materials, SM). Within the independent particle approximation, it can be expressed as

$$\begin{aligned} & \chi_{ab}^{i,B}(0; \omega, -\omega) \\ &= -\frac{\mu_B e^2 V_{\text{u.c.}}}{\hbar^2 \omega^2} \int \frac{d\mathbf{k}}{(2\pi)^3} \sum_{mnl} \frac{f_{lm} v_{lm}^a}{\omega_{ml} - \omega + i/\tau} \left( \frac{B_{mn}^i v_{nl}^b}{\omega_{mn} + i/\tau} - \frac{v_{mn}^b B_{nl}^i}{\omega_{nl} + i/\tau} \right) \end{aligned} \quad (2)$$

We have omitted the  $\mathbf{k}$ -dependence of the quantities in the integrand.  $\mu_B$ ,  $e$  and  $\hbar$  are Bohr magneton, electron charge and reduced Planck constant, respectively. Here we multiply unit cell volume ( $V_{\text{u.c.}}$ ) and  $\chi_{ab}^{i,B}$  corresponds to the magnetization in a unit cell.  $f_{lm} = f_l - f_m$  and  $\hbar\omega_{lm} = \hbar(\omega_l - \omega_m)$  are the difference between equilibrium occupation number and band energy between bands  $|l\rangle$  and  $|m\rangle$ , respectively.  $\mathbf{v}_{nl} = \langle n|\hat{\mathbf{v}}|l\rangle$  is the velocity matrix. For the spin and orbital contributions, one can set  $\mathbf{B}_{mn} = 2\mathbf{S}_{mn} = 2\langle m|\mathbf{S}|n\rangle$  and  $\mathbf{B}_{mn} = \mathbf{L}_{mn} = \langle m|\mathbf{L}|n\rangle$ , where  $\mathbf{S}$  and  $\mathbf{L}$  are spin and orbital angular momentum operators, respectively. The carrier lifetime  $\tau$  is set to be 0.2 ps in the following. We define symmetric real and asymmetric imaginary parts of Eq. (2) as

$$\begin{aligned} \eta_{ab}^{i,B} &= \frac{1}{2} \text{Re}\{\chi_{ab}^{i,B} + \chi_{ba}^{i,B}\} \\ \xi_{ab}^{i,B} &= \frac{1}{2} \text{Im}\{\chi_{ab}^{i,B} - \chi_{ba}^{i,B}\} \end{aligned} \quad (3)$$

which correspond to the response function under LPL and circularly polarized light (CPL), respectively.

Eq. (2) describes a three-band process, as illustrated in Figure 1b. The virtual transition between band  $m$  and  $l$  is mediated by  $n$ . If on a  $\mathbf{k}$ -point, different bands have different spin/orbital polarization, then a net magnetization change  $\delta M^i$  can be established. One could use symmetry analysis to examine the response explicitly. Under spatial inversion  $\mathcal{P}$ , axial vectors  $M$ ,  $S$  and  $L$  are even, while polar vectors  $E$  and  $v$  are odd. From both Eqs. (1) and (2), one can deduce that the NLEE does not require  $\mathcal{P}$  breaking, in contrast to LEE or the bulk photovoltaic effect (BPVE), which vanish in  $\mathcal{P}$ -conserved systems. It is more intriguing to study the NLEE under time reversal operation  $\mathcal{T}$ . Under  $\mathcal{T}$  operation,  $M, S, L$  and  $v$  are odd, while  $E$  is even. Therefore, from Eq. (1) one may deduce that the NLEE should vanish in a  $\mathcal{T}$ -conserved system under LPL. However, Eq. (2) yields a contrary conclusion: One has  $\mathcal{T}B^i(\mathbf{k}) = -B^{i*}(-\mathbf{k})$  and  $\mathcal{T}v^a(\mathbf{k}) = -v^{a*}(-\mathbf{k})$ , where  $^*$  denotes the complex conjugate, hence contributions from  $\pm\mathbf{k}$  do not cancel, and  $\mathcal{T}$  does not enforce a zero  $\chi_{ab}^{i,B}$  (see also SM). Intuitively, LPL induces photocurrent with vorticity as it flows

pass atoms with chiral neighboring surroundings (crystal field), like eddy when water flows pass a rock in a stream, which generally lead to a net magnetization unless mirror symmetries are present, as we will show below (Figure 1c). In  $\mathcal{P}$ -broken systems, the vortex currents do not exactly cancel, and lead to a net charge current in the bulk, which is the BPVE. In  $\mathcal{P}$ -conserved systems, in the bulk the net charge current should vanish, but there is still a net current on the surfaces, where  $\mathcal{P}$  is naturally broken. The contradiction between Eqs. (1) and (2) can be resolved if one considers the dissipation. Light with above-bandgap frequencies can be absorbed by electron interband transitions and then dissipated. Such dissipation breaks  $\mathcal{T}$  of the light-matter system, according to the second law of thermodynamics. Actually, similar reasonings apply to the Ohm current. Under  $\mathcal{T}$ , charge current is odd, while the electric field is even. But the Ohm current does exist. This is because the Joule heating breaks  $\mathcal{T}$ , even if the material possesses  $\mathcal{T}$  in equilibrium.

In the following, we perform *ab initio* calculations to illustrate NLEE in various 2D materials that have large surface area-to-volume ratio and are easily optically accessible. We first use monolayer (ML) TMDs as an example to show that the orbital contribution to the magnetic moment can be significantly greater than the spin contribution in intrinsic nonmagnetic systems. Then we use bilayer (BL) TMDs to show that different magnetic orderings can be obtained under LPL, depending on the interlayer stacking symmetry. Finally, we take 2D AFM material CrI<sub>3</sub> to discuss the possible AFM order manipulation under NLEE.

**Monolayer MoTe<sub>2</sub>: Spin and Orbital Contributions.** For the spontaneous magnetization in magnetic materials, the contribution from the orbital degree of freedom is usually weaker than that from the spin degree of freedom. This is due to the orbital quenching by strong crystal field, that causes the orbital contribution to be typically less than 10% of the total  $m = \mu_B(2S + L)$ <sup>25</sup>. On the contrary, for the non-equilibrium magnetization, we will show that the orbital angular momentum could contribute more significantly than the spin angular momentum, due to ironically the chirality of the same strong crystal field.

As an example, we use 2H TMDs (MoTe<sub>2</sub>), which exhibit many peculiar properties and are widely studied in recent years. Particularly, ML 2H TMDs (Figure 2a) possesses mirror symmetries  $\mathcal{M}_x$  and  $\mathcal{M}_z$ . Notably,  $\mathcal{M}_z$  enforces Zeeman type (out-of-plane) spin/orbital texture.

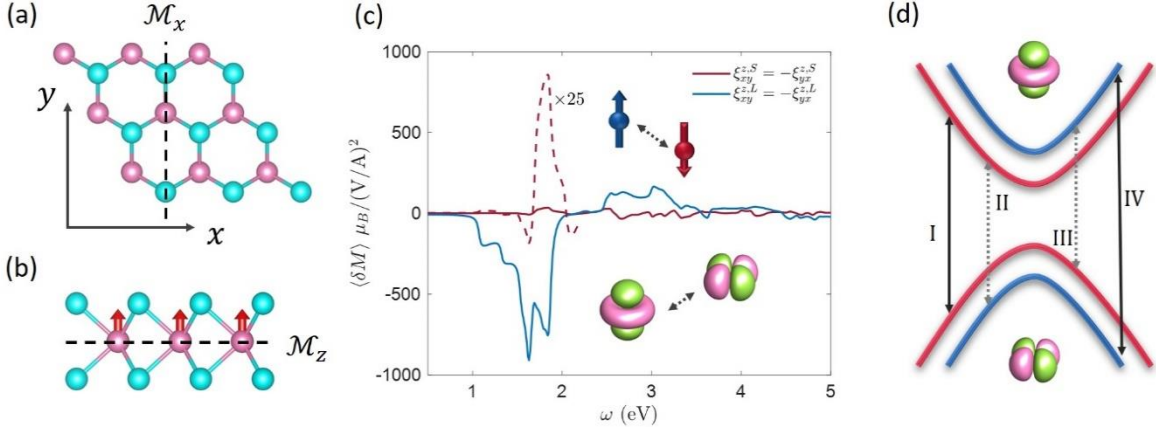


**Figure 2** (a, b) Top and Side view of ML MoTe<sub>2</sub>. The mirror symmetries are indicated by dashed line. The red arrows in (b) denotes the magnetization under CPL. (b) Orbital (blue) and spin (red) contributions to the total NLEE under CPL. The dash red curve  $\xi_{xy}^{z,S}$  is amplified by 25 times for  $\omega < 2.2$  eV. (d) Schematic spin and orbital projected band structure of MoTe<sub>2</sub> near K point. Blue (red) indicates spin up (down) states, while the VB (CB) have major contribution from  $d_{-2}$  ( $d_0$ ) orbitals. I-IV denote four possible interband transitions.

Here we could examine the constrains on NLEE from mirror symmetries. The polar vector  $\mathbf{E}$  satisfies  $\mathcal{M}_j E^a = (-1)^{\delta_{ja}} E^a$ , while the axial vector  $\mathbf{B}$  gives  $\mathcal{M}_j B^i = -(-1)^{\delta_{ji}} B^i$ . Consequently, in systems with  $\mathcal{M}_j$ ,  $\chi_{ab}^{i,B}$  would vanish if  $\delta_{ji} + \delta_{ja} + \delta_{jb}$  is even. Specific to ML MoTe<sub>2</sub>, with in-plane electric field, the only non-vanishing component of the NLEE tensor is  $\chi_{xy}^{z,B}$ . Note that if  $\mathcal{M}_z$  is broken (e.g., by an electric field or in a Janus structure), then in-plane magnetization should exist.

Here we focus on CPL responses and plot  $\xi_{xy}^{z,B}$  (Figure 2b). A prominent feature is that the orbital part  $\xi_{xy}^{z,L}$  is about 25 times greater than the spin part  $\xi_{xy}^{z,S}$ . In other words, under CPL, the NLEE comes mostly from the orbital contribution. This phenomenon can be better understood when we assume a sufficiently long relaxation time ( $\tau \rightarrow \infty$ ) and use the two-band approximation, then we can rewrite Eqs. (2,3) as (see SM)

$$\begin{aligned} & \xi_{ab}^{i,B}(0; \omega, -\omega) \\ &= \tau \frac{\pi \mu_B e^2 V_{\text{u.c.}}}{2 \hbar^2} \int \frac{d\mathbf{k}}{(2\pi)^3} \sum_{m \neq l} f_{lm} [r_{lm}^a, r_{ml}^b] (B_{mm}^i - B_{ll}^i) \delta(\omega_{ml} - \omega) \end{aligned} \quad (4)$$

Here  $[r_{lm}^a, r_{ml}^b] = r_{lm}^a r_{ml}^b - r_{lm}^b r_{ml}^a$  is the interband Berry curvature, while  $\Delta B_{ml}^i = B_{mm}^i - B_{ll}^i$  is the difference between the spin/orbital polarization on band  $m$  and  $l$ . This formalism is illustrated

on the right side of Figure 1b. We schematically plot the band structure of MoTe<sub>2</sub> near the K valley in Figure 2c, while the K' valley can be similarly analyzed. The Zeeman type spin splitting induced by SOC is indicated by the red (spin up) and blue (spin down) color. Note that the orbital character is mostly determined by crystalline field, thus SOC does not significantly change it. The valance bands (VB) and conduction bands (CB) have major contributions from  $d_{-2} = \frac{1}{\sqrt{2}}(d_{x^2-y^2} - id_{xy})$  and  $d_0 = d_{z^2}$  orbitals, respectively (SM). There are four possible interband transitions, indicated by I – IV in Figure 2b. II and III have sizable  $\Delta S^z$ , but they are anti-parallel, so one has  $\xi_{xy}^{z,S} \sim \text{II} - \text{III}$ . As for the orbital part, all I – IV contributes to  $\Delta L^z$ , thus  $\xi_{xy}^{z,L} \sim \text{I} + \text{II} + \text{III} + \text{IV}$ . Furthermore, since II and III flip spin, their transition rate should be much lower than I and IV. Therefore, in general one would have  $\xi_{xy}^{z,L} \gg \xi_{xy}^{z,S}$ . In fact, the orbital texture leads to non-zero  $\xi_{xy}^{z,L}$ , and is then transmitted to spin texture by SOC, which leads to a finite  $\xi_{xy}^{z,S}$ <sup>26</sup>. Without SOC, the spin-rotation symmetry is conserved, and the two VBs and CBs are degenerate (no spin splitting). In this case,  $\xi_{xy}^{z,S}$  vanishes, whereas  $\xi_{xy}^{z,L}$  persists (SM).

We now briefly compare the NLEE and LEE magnitudes. The peak value of  $\xi_{xy}^{z,T}$  is one the order of  $10^3 \mu_B / \left(\frac{V}{\text{\AA}}\right)^2$ . We also calculate the LEE response function  $\zeta_a^i$  of MoTe<sub>2</sub>, which exists only when the Fermi level  $\mathcal{E}_F$  is tuned into the VB or CB. When  $\mathcal{E}_F$  is 0.2 eV inside the VB or CB,  $\zeta_a^i$  is on the order of  $0.1 \sim 1 \mu_B / \frac{V}{\text{\AA}}$  (SM). This indicates that with  $E \gtrsim 10$  MV/m, the NLEE strength would exceed that of LEE.

**Bilayer MoTe<sub>2</sub>: Stacking dependent magnetic orders.** The magnetization of ML MoTe<sub>2</sub> exhibits an in-plane FM ordering. On the other hand, in multi-layer or multi-sublattice systems, the interplay between the layers or the sublattices can lead to various magnetization orderings, including AFM and FM. Here we use BL MoTe<sub>2</sub> as an example. Note that  $\mathcal{M}_z$  can be broken in BL TMDs. When  $\mathcal{M}_z$  exists, the total in-plane magnetization should be zero, but there still can be a *local* hidden in-plane magnetization under LPL.

Three high symmetry stacking patterns of BL MoTe<sub>2</sub> are shown in Figure 3. In AA stacking (Figure 3a), Mo (Te) atoms of the upper layer sit directly above Mo (Te) atoms of the lower layer, leading to an inter-layer mirror symmetry  $\mathcal{M}_z$ . In AA' stacking (Figure 3d), Mo (Te) atoms in the

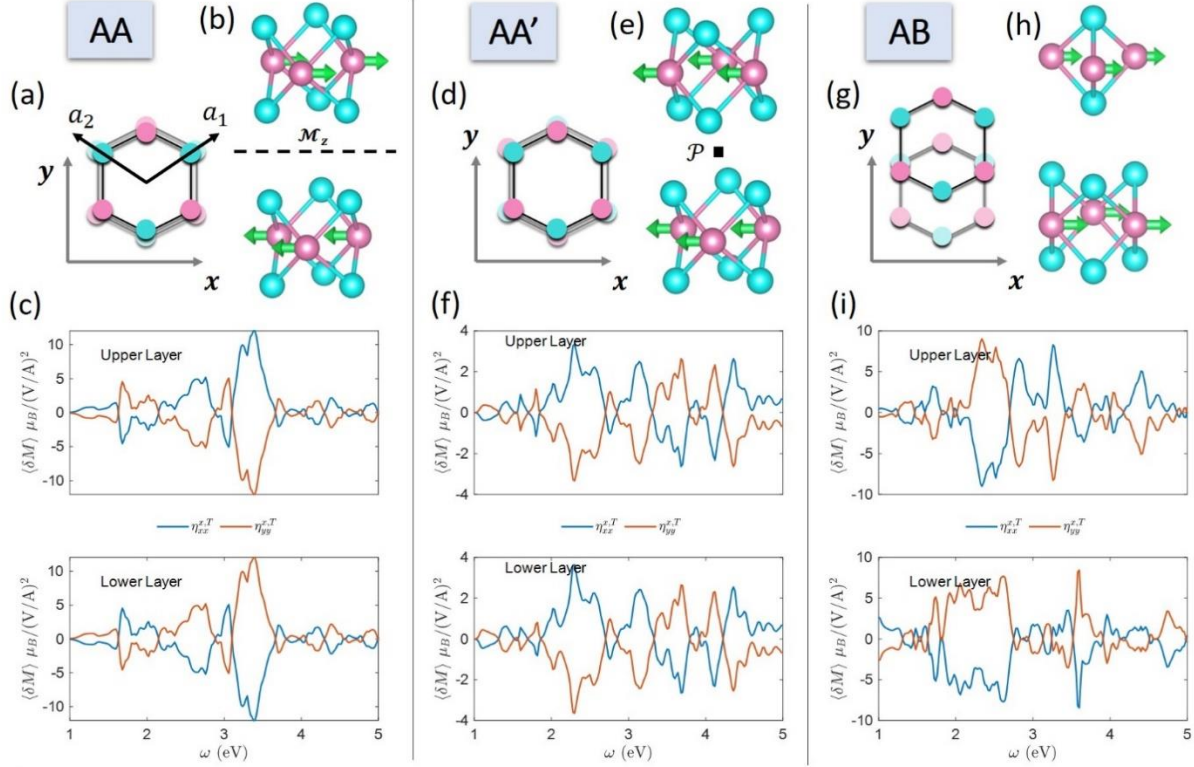


**Figure 3** The NLEE under LPL of BL MoTe<sub>2</sub> with AA (left), AA' (middle) and AB (right column). (a,d,e) are skematic plots of the stacking pattern. (b,e,h) show the magnetic order under LPL with the green arrows indicate the NLEE magnetization. Pink: Mo; Cyan: Te. (c,f,i) show the response function  $\eta_{xx}^{x,T} = -\eta_{yy}^{x,T}$ .

upper layer are above the Te (Mo) atoms in the lower layer, and there is an inter-layer inversion symmetry  $\mathcal{P}$ . Finally, the AB stacking (Figure 3g) has neither  $\mathcal{M}_z$  nor  $\mathcal{P}$ .

The response function  $\eta_{xx}^{x,T} = -\eta_{yy}^{x,T}$  are shown in the lower panels of Figure 3. Note that different from  $\xi^T$ , under LPL  $\eta^T$  has comparable contributions from  $\eta^S$  and  $\eta^L$  (SM). One can see that the opto-magnetic ordering is strongly dependent on the stacking pattern. For AA stacking, the magnetization on the upper and lower layers are exactly anti-parallel, leading to an AFM ordering. For AA' stacking, the two layers exhibit parallel magnetization, which can be considered as an FM ordering. Finally, for the AB stacking,  $\eta^T$  on the upper and lower layers do not exhibit a simple relationship, and staggered magnetism is thus expected. The magnetic orderings of different stacking patterns come from symmetry constraints. For example, the inter-layer  $\mathcal{M}_z$  of AA stacking swaps the two layers and flips  $M^x$ . Consequently, local  $M^x$  associated with the two layers must be the opposite. Actually, this effect is also manifested in the layer-projected  $\mathbf{k}$ -space spin/orbital texture  $P_l B_{mm}^x(\mathbf{k}) P_l$  (see Methods), as shown in Figure 4a for the highest VB. One can

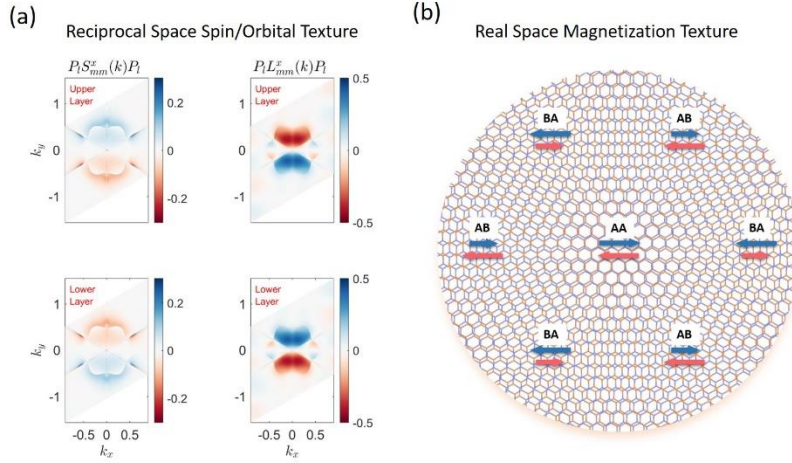


**Figure 4** (a) Reciprocal space local spin/orbital texture  $P_l B_{mm}^x(\mathbf{k}) P_l$  for the highest VB on the upper and lower layer of BL MoTe<sub>2</sub>. The left (right) column is the spin (orbital) texture. (b) Real space magnetization texture on a Moiré pattern. The blue and pink arrows indicate magnetization on the upper and lower layers, respectively.

see that for any  $\mathbf{k}$ -point, the textures on the upper and lower layers are exactly opposite to each other. In equilibrium states, the spin/orbital polarization of all occupied states sum up to zero, hence local spin/orbital polarizations are *hidden*<sup>20</sup>. However, when the system is driven out of equilibrium, the hidden magnetization would emerge, and an AFM magnetization appears. Similar reasonings apply to AA' stacking pattern, where  $\mathcal{P}$  enforces FM ordering. As for AB' stacking, there are no inter-layer symmetry constraints, hence the magnetizations on the two layers are not directly correlated. Interestingly, when the two layers are twisted to form a Moiré pattern, a real-space spin texture can be created. The Moiré pattern exhibits spatially varying stacking patterns, which leads to spatially varying magnetic orderings with NLEE (Figure 4b). Also, the non-equilibrium magnetization can be either (anti)-parallel or perpendicular to the electric field, which may lead to interesting physical phenomena. Particularly, the (anti)-parallel electric and magnetic field can be regarded as a nonlinear axion coupling<sup>27</sup>.

**CrI<sub>3</sub>: AFM Order Manipulation.** Until now, we have been discussing non-magnetic materials, where the spontaneous magnetization  $M^0$  is zero, and a non-equilibrium steady-state magnetization  $\delta M$  is generated under light. This can be considered as a non-magnetic to magnetic transition. On the other hand, in magnetic materials there is already finite spontaneous magnetization  $M^0$  in equilibrium. Light illumination could induce an additional non-equilibrium

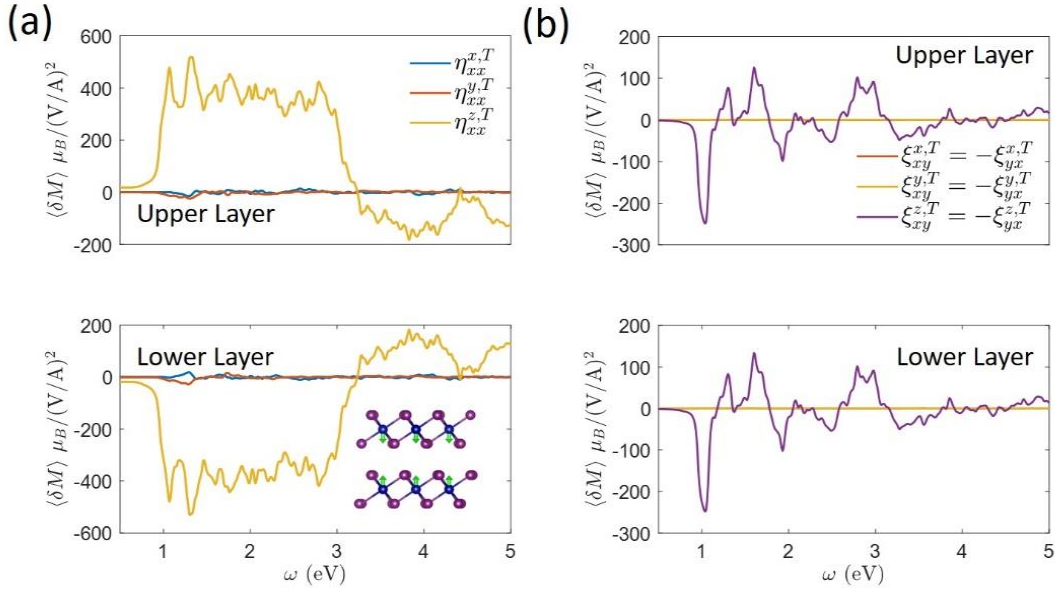


**Figure 5** NLEE of AFM CrI<sub>3</sub> with magnetization along z axis. Under (a) LPL and (b) CLP, the NLEE magnetization are opposite and parallel on the two layers, respectively. Inset of (a): atomic structure of BL CrI<sub>3</sub>. The green arrows indicate the equilibrium magnetization.

magnetization  $\delta M$  under NLEE. This  $\delta M$  can be considered as an effective magnetic field  $H_{\text{eff}}$ , which exerts forces on  $M^0$ . Previous studies based on LEE suggest that this  $H_{\text{eff}}$  can cause the magnetic moment precession, and a magnetic phase transition may occur when  $H_{\text{eff}}$  is strong enough<sup>28–30</sup> with a pulsed light. Recently, the AFM spintronics<sup>31–33</sup> has attracted great interest. Compared with FM materials, using AFM materials has several advantages, such as the insensitivity to external field, the absence of stray field, and the fast dynamics with terahertz frequency, etc. Manipulating the magnetic ordering of AFM materials requires that the effective field on the two magnetic sublattices are opposite so that no net magnetization is induced. Obviously, this cannot be achieved with a static external magnetic field. A few approaches has been proposed to manipulate AFM ordering, such as electrical approaches based on LEE<sup>34–36</sup>, and optical approaches<sup>33</sup> based on IFE<sup>37</sup> or the Zeeman coupling with a THz light<sup>38</sup>.

Here we propose that NLEE can be an alternative methodology for manipulating AFM ordering. Compared with LEE, NLEE is applicable to semiconductors, and the choice of light frequency, polarization, and intensity could provide good flexibility. Furthermore, the ultra-fast ultra-strong pulsed lasers render it possible to manipulate the AFM ordering, and even trigger AFM order switching (i.e.,  $M^0 \rightarrow -M^0$ ) on a picosecond timescale. To illustrate the NLEE in

magnetic materials, we take bilayer  $\text{CrI}_3$  as an example. The magnetic ground state of bilayer  $\text{CrI}_3$  is AFM with the easy axis along the  $z$  direction. To be specific, we assume that  $M^0$  on the upper (lower) layer point downwards (upwards). The response functions  $\eta$  and  $\xi$  under this configuration are plotted in Figure 5, where a positive (negative) value of  $\eta$  and  $\xi$  indicates a  $\delta M$  along  $+z$  ( $-z$ ) direction. One can see the under CPL,  $\delta M$  on the two layers are parallel to each other, whereas under LPL they are (approximately) anti-parallel. Notably, for  $\omega \gtrsim 3$  eV,  $\delta M$  is opposite to  $M^0$ , which can be utilized to swap the magnetization and trigger an AFM order switching. We estimate the effective magnetic field from  $H_{\text{eff}} = \frac{\delta M J_{\text{ex}}}{(\mu_B)^2}$ , where  $J_{\text{ex}}$  is the exchange energy between carrier spin and the local magnetic moment, and is estimated to be  $\sim 1$  eV from band structures (see SM. For an order-of-magnitude estimation, here we assume that carrier orbital and spin magnetization have identical exchange energy with local magnetic moment).  $\eta$  is on the order of  $100 \mu_B / \left(\frac{V}{\text{\AA}}\right)^2$ , and one has  $H_{\text{eff}} \sim 10^6 \text{ T} / \left(\frac{V}{\text{\AA}}\right)^2$ . Therefore, an electric field  $E \sim 0.1 \text{ MV/cm}$  (corresponding to light intensity  $\sim 27 \text{ MW/cm}^2$ ) could generate an  $H_{\text{eff}} \sim 1 \text{ T}$ , which is strong enough to trigger a magnetic order transition in  $\text{CrI}_3$ <sup>3</sup>. The temperature increase under such light illumination is estimated to be on the order of 10 K (see SM), thus  $\text{CrI}_3$  can be kept below its Néel temperature, which is around 45 K<sup>39,40</sup>.

**Discussions and Conclusions.** First, we would like to discuss the relationship between NLEE and IFE<sup>15,16</sup> and ICME<sup>17-19</sup>, which also generate an effective magnetic field  $H_{\text{eff}}$  under CPL and LPL, respectively. Phenomenologically, IFE and ICME come from the derivative of the light-matter interaction Hamiltonian  $\mathcal{H}_{\text{int}} = \frac{1}{2} \varepsilon_{ab} E_a E_b^*$  with respect to magnetization, i.e.,  $H_k = \frac{\partial \mathcal{H}_{\text{int}}}{\partial M_k} = \frac{1}{2} \frac{\partial \varepsilon_{ab}}{\partial M_k} E_a E_b^*$ <sup>19,30</sup>. Here  $\varepsilon_{ab}$  is the dielectric function. Due to the symmetry constraints<sup>41</sup>, to the lowest order  $\varepsilon$  satisfies  $\varepsilon_{ab}^{(a)} = \alpha_{abk} M_k^0$  and  $\varepsilon_{ab}^{(s)} = \varepsilon_{ab}^0 + \frac{1}{2} \beta_{abkl} M_k^0 M_l^0$ , where  $\varepsilon^0$  is vacuum permittivity, while  $\varepsilon^{(a)} / \varepsilon^{(s)}$  are the asymmetric/symmetric part of  $\varepsilon$ .  $\alpha_{abk}$  and  $\beta_{abkl}$  are phenomenological parameters. Thus, one has  $H_k^{\text{IFE}} \propto \alpha_{abk} (E_a E_b^* - E_b E_a^*)$  and  $H_k^{\text{ICME}} \propto \beta_{abkl} M_l^0 (E_a E_b^* + E_b E_a^*)$ . Consequently, in non-magnetic materials ( $M^0 = 0$ ) IFE can exist, while ICME must vanish. On the other hand, NLEE, which generates non-equilibrium magnetization  $\delta M$ , can be understood as the derivative of  $\mathcal{H}_{\text{int}}$  with respect to magnetic field, i.e.,  $\delta M_k = \frac{1}{2} \frac{\partial \varepsilon_{ab}}{\partial H_k} E_a E_b^*$ . Since  $H$  and  $M$  are conjugate variables, NLEE and IFE/ICME can be regarded as two

complementary perspectives on the same magneto-optic effect. Notably, our quantum theory provides an approach to calculate the response function  $\chi_{ab}^{i,B}$  with *ab initio* calculation, whereas  $\alpha_{abk}$  and  $\beta_{abkl}$ , to the best of our knowledge, cannot yet be calculated directly. In addition, we clarify that the magnetization  $\delta M$ , or equivalently the effective field  $H_{\text{eff}}$ , can be generated under LPL with above-bandgap frequencies in nonmagnetic materials, in contrast to the conclusion from the phenomenological analysis on ICME, where  $H_k^{\text{ICME}}$  should be zero when  $M_l^0$  is zero. The reciprocity is broken by dissipation and the NLEE can be regarded as a non-reciprocal process.

Second, the spin dynamics of AFM materials such as  $\text{CrI}_3$  under NLEE remains to be studied. Note that under LPL, one has  $\delta M_k \propto H_k^{\text{ICME}} \propto \beta_{abkl} M_l^0 (E_a E_b^* + E_a^* E_b)$ . When the magnetic anisotropy is not too strong, it is reasonable to assume that the off-diagonal terms ( $k \neq l$ ) of  $\beta_{abkl}$  are much smaller than the diagonal terms ( $k = l$ ), thus  $H$  should be approximately (anti)-parallel to  $M^0$ , which is verified by our *ab initio* calculations (SM). The spin dynamics under  $H$  with such a pattern shall be studied carefully to determine whether it is possible to trigger AFM order switching, and if possible, to determine the optimal light pulse intensity, duration, etc.

In conclusion, we develop the quantum theory of nonlinear Edelstein effect. We elucidate that orbital- and spin-magnetization could emerge even in nonmagnetic materials under LPL irradiation, and different opto-magnetic orderings are realizable in multi-layer or multi-sublattice systems. This approach could also effectively manipulate magnetic ordering in semiconducting and insulating magnetic materials, which can serve as an alternative of linear Edelstein effect, which is applicable only in metals.

**Methods.** The Vienna *ab initio* simulation package (VASP)<sup>42,43</sup> is used for the first-principles calculations based on density functional theory (DFT)<sup>44,45</sup>. The exchange-correlation interactions are treated by the generalized gradient approximation (GGA) in the form of Perdew-Burke-Ernzerhof (PBE)<sup>46</sup>. Projector augmented wave (PAW) method<sup>47</sup> and plane-wave basis functions are used to treat the core and valence electrons, respectively. For DFT calculations, the first Brillouin zone is sampled by a  $\Gamma$ -centered  $\mathbf{k}$ -mesh with grid density of at least  $2\pi \times 0.02 \text{ \AA}^{-1}$  along each dimension. The DFT+ $U$  method is adopted to treat the  $d$  orbitals of spin polarized Cr atoms in  $\text{CrI}_3$  ( $U = 3.0 \text{ eV}$ ). Tight-binding orbitals are generated from Bloch waves in DFT

calculations, using the Wannier90 package<sup>48</sup>. The tight-binding Hamiltonian is then used to interpolate the band structure on a much denser  $\mathbf{k}$ -mesh calculate the LEE and NLEE response functions. This  $\mathbf{k}$ -mesh convergence is well tested. In order to calculate the real space local magnetization, we define a projection operator  $P_l = \sum_{i \in l} |\psi_i\rangle\langle\psi_i|$ , where  $l$  denotes the spatial region (e.g.,  $l$ -th layer in a multi-layer system, or the  $l$ -th sublattice in a multi-sublattice system), while  $|\psi_i\rangle$  is the tight binding orbital belonging to region  $l$ . Then the operator  $P_l B P_l$  is to replace  $B$  operator in Eq. (2). We simply used atomic orbitals (s, p, d, etc.) to calculate the orbital angular momentum ( $B = L$ ). So only the contribution from intra-atom term  $\langle n\mathbf{R} | \mathbf{r} \times \mathbf{p} | m\mathbf{R} \rangle$  is included, while the contribution from inter-atom term  $\langle n\mathbf{R} | \mathbf{r} \times \mathbf{p} | m\mathbf{R}' \rangle$  is neglected.

### Acknowledgments.

This work was supported by an Office of Naval Research MURI through grant #N00014-17-1-2661. We are grateful to discussions with Zhurun Ji.

### References

1. Žutić, I., Fabian, J. & Sarma, S. Das. Spintronics: Fundamentals and applications. *Reviews of Modern Physics* **76**, 323–410 (2004).
2. Bader, S. D. & Parkin, S. S. P. Spintronics. *Annu. Rev. Condens. Matter Phys.* **1**, 71–88 (2010).
3. Huang, B. *et al.* Electrical control of 2D magnetism in bilayer CrI<sub>3</sub>. *Nat. Nanotechnol.* **13**, 544–548 (2018).
4. Edelstein, V. M. Spin polarization of conduction electrons induced by electric current in two-dimensional asymmetric electron systems. *Solid State Commun.* **73**, 233–235 (1990).
5. Sánchez, J. C. R. *et al.* Spin-to-charge conversion using Rashba coupling at the interface between non-magnetic materials. *Nat. Commun.* **4**, 1–7 (2013).
6. Zhang, H. J. *et al.* Charge-to-spin conversion and spin diffusion in Bi/Ag bilayers observed by spin-polarized positron beam. *Phys. Rev. Lett.* **114**, 166602 (2015).
7. Rojas-Sánchez, J. C. *et al.* Spin to Charge Conversion at Room Temperature by Spin Pumping into a New Type of Topological Insulator:  $\alpha$ -Sn Films. *Phys. Rev. Lett.* **116**, 096602 (2016).
8. Ralph, D. C. & Stiles, M. D. Spin transfer torques. *J. Magn. Magn. Mater.* **320**, 1190–1216 (2008).
9. Sinova, J., Valenzuela, S. O., Wunderlich, J., Back, C. H. & Jungwirth, T. Spin Hall effects. *Rev. Mod. Phys.* **87**, 1213–1260 (2015).
10. D’Yakonov, M. I., Perel’, V. I., D’Yakonov, M. I. & Perel’, V. I. Possibility of Orienting Electron Spins with Current. *JETPL* **13**, 467 (1971).

11. Dyakonov, M. I. & Perel, V. I. Current-induced spin orientation of electrons in semiconductors. *Phys. Lett. A* **35**, 459–460 (1971).
12. Ando, K. *et al.* Inverse spin-Hall effect induced by spin pumping in metallic system. in *Journal of Applied Physics* **109**, 103913 (American Institute of PhysicsAIP, 2011).
13. Xu, H., Wang, H., Zhou, J. & Li, J. Pure Spin Photocurrent in Non-centrosymmetric Crystals: Bulk Spin Photovoltaic Effect. (2020).
14. Fei, R., Lu, X. & Yang, L. Intrinsic Spin Photogalvanic Effect in Nonmagnetic Insulator. (2020).
15. Battiato, M., Barbalinardo, G. & Oppeneer, P. M. Quantum theory of the inverse Faraday effect. *Phys. Rev. B - Condens. Matter Mater. Phys.* **89**, 014413 (2014).
16. Popova, D., Bringer, A. & Blügel, S. Theory of the inverse Faraday effect in view of ultrafast magnetization experiments. *Phys. Rev. B - Condens. Matter Mater. Phys.* **84**, 214421 (2011).
17. Gridnev, V. N. Phenomenological theory for coherent magnon generation through impulsive stimulated Raman scattering. *Phys. Rev. B - Condens. Matter Mater. Phys.* **77**, 094426 (2008).
18. Kalashnikova, A. M. *et al.* Impulsive excitation of coherent magnons and phonons by subpicosecond laser pulses in the weak ferromagnet FeBO<sub>3</sub>. *Phys. Rev. B - Condens. Matter Mater. Phys.* **78**, 104301 (2008).
19. Iida, R. *et al.* Spectral dependence of photoinduced spin precession in DyFeO<sub>3</sub>. *Phys. Rev. B - Condens. Matter Mater. Phys.* **84**, 064402 (2011).
20. Zhang, X., Liu, Q., Luo, J. W., Freeman, A. J. & Zunger, A. Hidden spin polarization in inversion-symmetric bulk crystals. *Nat. Phys.* **10**, 387–393 (2014).
21. Degen, C. L., Reinhard, F. & Cappellaro, P. Quantum sensing. *Rev. Mod. Phys.* **89**, 035002 (2017).
22. Kraut, W. & Von Baltz, R. Anomalous bulk photovoltaic effect in ferroelectrics: A quadratic response theory. *Phys. Rev. B* **19**, 1548–1554 (1979).
23. Von Baltz, R. & Kraut, W. Theory of the bulk photovoltaic effect in pure crystals. *Phys. Rev. B* **23**, 5590–5596 (1981).
24. Gao, Y., Wang, C. & Xiao, D. Topological Inverse Faraday Effect in Weyl Semimetals. (2020).
25. Dresselhaus, M. S. *SOLID STATE PHYSICS PART III Magnetic Properties of Solids*.
26. Go, D., Jo, D., Kim, C. & Lee, H. W. Intrinsic Spin and Orbital Hall Effects from Orbital Texture. *Phys. Rev. Lett.* **121**, 086602 (2018).
27. Wilczek, F. Two applications of axion electrodynamics. *Phys. Rev. Lett.* **58**, 1799–1802 (1987).
28. Stanciu, C. D. *et al.* All-optical magnetic recording with circularly polarized light. *Phys. Rev. Lett.* **99**, 047601 (2007).
29. Kirilyuk, A., Kimel, A. V. & Rasing, T. Ultrafast optical manipulation of magnetic order. *Rev. Mod. Phys.* **82**, 2731–2784 (2010).
30. Kimel, A. V. & Zvezdin, A. K. Magnetization dynamics induced by femtosecond light pulses. *Low Temp. Phys.* **41**, 682–688 (2015).
31. Baltz, V. *et al.* Antiferromagnetic spintronics. *Rev. Mod. Phys.* **90**, 015005 (2018).
32. Jungwirth, T., Marti, X., Wadley, P. & Wunderlich, J. Antiferromagnetic spintronics. *Nature*

- Nanotechnology* **11**, 231–241 (2016).
33. Němec, P., Fiebig, M., Kampfrath, T. & Kimel, A. V. Antiferromagnetic opto-spintronics. *Nature Physics* **14**, 229–241 (2018).
  34. Železný, J. *et al.* Relativistic néel-order fields induced by electrical current in antiferromagnets. *Phys. Rev. Lett.* **113**, 157201 (2014).
  35. Železný, J. *et al.* Spin-orbit torques in locally and globally noncentrosymmetric crystals: Antiferromagnets and ferromagnets. *Phys. Rev. B* **95**, 014403 (2017).
  36. Salemi, L., Berritta, M., Nandy, A. K. & Oppeneer, P. M. Orbitally dominated Rashba-Edelstein effect in noncentrosymmetric antiferromagnets. *Nat. Commun.* **10**, 1–10 (2019).
  37. Kimel, A. V. *et al.* Inertia-driven spin switching in antiferromagnets. *Nat. Phys.* **5**, 727–731 (2009).
  38. Wienholdt, S., Hinzke, D. & Nowak, U. THz switching of antiferromagnets and ferrimagnets. *Phys. Rev. Lett.* **108**, 247207 (2012).
  39. Huang, B. *et al.* Layer-dependent ferromagnetism in a van der Waals crystal down to the monolayer limit. *Nature* **546**, 270–273 (2017).
  40. Seyler, K. L. *et al.* Ligand-field helical luminescence in a 2D ferromagnetic insulator. *Nat. Phys.* **14**, 277–281 (2018).
  41. Kubo, R. Statistical’Mechanical Theory of Irreversible Processes. I. General Theory and Simple Applications to Magnetic and Conduction Problems. *J. Phys. Soc. Japan* **12**, 570–586 (1957).
  42. Kresse, G. & Furthmüller, J. Efficiency of ab-initio total energy calculations for metals and semiconductors using a plane-wave basis set. *Comput. Mater. Sci.* **6**, 15–50 (1996).
  43. Kresse, G. & Furthmüller, J. Efficient iterative schemes for *ab initio* total-energy calculations using a plane-wave basis set. *Phys. Rev. B* **54**, 11169–11186 (1996).
  44. Hohenberg, P. & Kohn, W. Inhomogeneous Electron Gas. *Phys. Rev.* **136**, B864–B871 (1964).
  45. Kohn, W. & Sham, L. J. Self-Consistent Equations Including Exchange and Correlation Effects. *Phys. Rev.* **140**, A1133–A1138 (1965).
  46. Perdew, J. P., Burke, K. & Ernzerhof, M. Generalized Gradient Approximation Made Simple. *Phys. Rev. Lett.* **77**, 3865–3868 (1996).
  47. Blöchl, P. E. Projector augmented-wave method. *Phys. Rev. B* **50**, 17953–17979 (1994).
  48. Mostofi, A. A. *et al.* An updated version of wannier90: A tool for obtaining maximally-localised Wannier functions. *Comput. Phys. Commun.* **185**, 2309–2310 (2014).